Direct Imaging of Dynamic Glassy Behavior in a Strained Manganite Film

Worasom Kundhikanjana,[1,2] Zhigao Sheng,[3,4,5] Yongliang Yang,[1] Keji Lai,[6] Eric Yue Ma,[1] Yong-Tao Cui,[1] Michael A. Kelly,[1] Masao Nakamura,[3] Masashi Kawasaki,[3,7] Yoshinori Tokura,[3,7] Qiaochu Tang,[8] Kun Zhang,[8] Xinxin Li,[8] and Zhi-Xun Shen[1,*]

[1]*Department of Applied Physics and Geballe Laboratory for Advanced Materials, Stanford University, Stanford, California 94305, USA*

[2]*School of Physics, Institute of Science, Suranaree University of Technology, Nakorn Ratchasima, Thailand*

[3]*RIKEN Center for Emergent Matter Science (CEMS), Wako 251-0198, Japan*

[4]*High Magnetic Field Laboratory of Chinese Academy of Science, Hefei 230031, China*

[5]*Collaborative Innovation Center of Advanced Microstructures, Nanjing University, Nanjing 210093, China*

[6]*Department of Physics, University of Texas at Austin, Austin, Texas 78712, USA*

[7]*Department of Applied Physics and Quantum Phase Electronics Research Center (QPEC), University of Tokyo, Tokyo 113-8656, Japan*

[8]*State Key Lab of Transducer Technology, Shanghai Institute of Microsystem and Information Technology, Chinese Academy of Sciences, Shanghai 200050, China*

(Received 21 July 2015; published 23 December 2015; corrected 30 December 2015)

Complex many-body interaction in perovskite manganites gives rise to a strong competition between ferromagnetic metallic and charge-ordered phases with nanoscale electronic inhomogeneity and glassy behaviors. Investigating this glassy state requires high-resolution imaging techniques with sufficient sensitivity and stability. Here, we present the results of a near-field microwave microscope imaging on the strain-driven glassy state in a manganite film. The high contrast between the two electrically distinct phases allows direct visualization of the phase separation. The low-temperature microscopic configurations differ upon cooling with different thermal histories. At sufficiently high temperatures, we observe switching between the two phases in either direction. The dynamic switching, however, stops below the glass transition temperature. Compared with the magnetization data, the phase separation was microscopically frozen, while spin relaxation was found in a short period of time.

DOI: 10.1103/PhysRevLett.115.265701 PACS numbers: 64.70.P-, 64.75.St

A glass is formed by rapid cooling of a viscous liquid, resulting in a supercooled liquid with no crystallinity [1]. Generally, such a supercooled state can occur in many systems with a first-order phase transition. In these systems, there are multiple competing states separated by a thermal barrier near the transition temperature. By rapid cooling, the system can be trapped in the nonfavorable state, resulting in slow relaxation and cooling-rate-dependent behaviors. Furthermore, the existence of complex energy landscapes often leads to different low-temperature states even under the same cooling process, known as nonergodicity. Perovskite manganites are a good example of systems with such dynamics. In half-doped manganites, the transition from the charge-ordered insulating state (CO-I) to the ferromagnetic metallic state (FM-M) is first order in nature, while the energetic proximity between the two crystalline states often results a phase separation [2,3] with one of states being metastable. The metastability gives rise to relaxation behaviors [4,5] and dependences on cooling histories [6–8]. Aspects of spin-glass-like behaviors are also found, such as frequency dependent ac susceptibility [9]. The phase-separated (PS) state is also highly susceptible to local parameters such as strain [10] and disorder [9].

Many models for manganite glass were constructed using macroscopic measurements [11]. However, the PS state is necessary for understanding the physics of manganites [2]. Transport measurements, therefore, have clear drawbacks. For example, macroscopic magnetization cannot distinguish intradomain relaxation from phase switching [12]. Although the dynamics of the PS state may be inferred from the transports through a manganite nanowire [13], these measurements are limited to a narrow temperature range with sufficient conductivity. To date, the PS state with distinct physical properties has been visualized by various microscopy techniques such as scanning tunneling microscopy [14], electron microscopy [15], photoemission spectroscopy [16], magnetic force microscopy [17,18], and, recently, near-field microwave impedance microscopy (MIM) [19]. However, most of these studies focus on the static phase separation. Direct visualization of the dynamic behaviors in the PS manganites is yet to be addressed.

In this Letter, we present the results of a MIM study on a $Pr_{0.55}(Ca_{0.75}Sr_{0.25})_{0.45}MnO_3$ (PCSMO) film. The high contrast between the two electrically distinct phases allows for a detailed study of the PS states. The large field of view and the high measurement stability enable tracking of the dynamic behavior of several FM-M domains in a wide temperature

range and after different thermal histories. The strong dependence on cooling history and measurement time for the microscopic configurations of this PS film showed the nonergodicity and relaxation behavior. Moreover, the dynamics of glassy behavior, driven and strongly influenced by strain, stop evolving below the freezing temperature.

The sample is a 40-nm-thick PCSMO [20–23] film grown on a (110) $(LaAlO_3)_{0.3}(SrAl_{0.5}Ta_{0.5}O_3)_{0.7}$ (LSAT) substrate by pulse laser deposition. In the x-ray reciprocal maps, the (222) and (310) peaks of the film align with those of the LSAT substrate, indicating a coherent growth [Fig. 1(a)]. Atomic force microscopy imaging of the film shows a flat surface with atomic steps [Fig. 1(a), inset] and sporadic Mn_3O_4 precipitates. At zero magnetic (B) field, the resistivity measurement shows an insulating behavior at all temperatures [dotted red curve in Fig. 1(b)], with a transition from PM-I to CO-I at $T_{co} = 200$ K (see the Supplemental Material [24] for details). The FM-M state, on the other hand, can be easily recovered by application of a small $B \sim 1$ T [Fig. 1(b), solid black]. A large hysteresis between the zero field cooling (ZFC) and field warm curve, noticeable in both resistivity [Fig. 1(b)] and the magnetization curves (Supplemental Material [24]), suggests the existence of a PS state. Note that by growing the film on another substrate, $CaTiO_3/SrTiO_3$ (CTO/STO), with a lattice constant of 3.826 Å that is closer to the bulk PCSMO film than LSAT (3.869 Å) [25], the film becomes metallic at low temperature [Fig. 1(b), dashed blue]. The transport behavior of PCSMO/LSAT is similar to bulk $(La, Pr)_{0.625}Ca_{0.375}MnO_3$ [6–8,17], where the glassy PS state is found. Unlike bulk manganites with accommodation strains [17], the PS in epitaxial films is strongly influenced by the strain from the substrate.

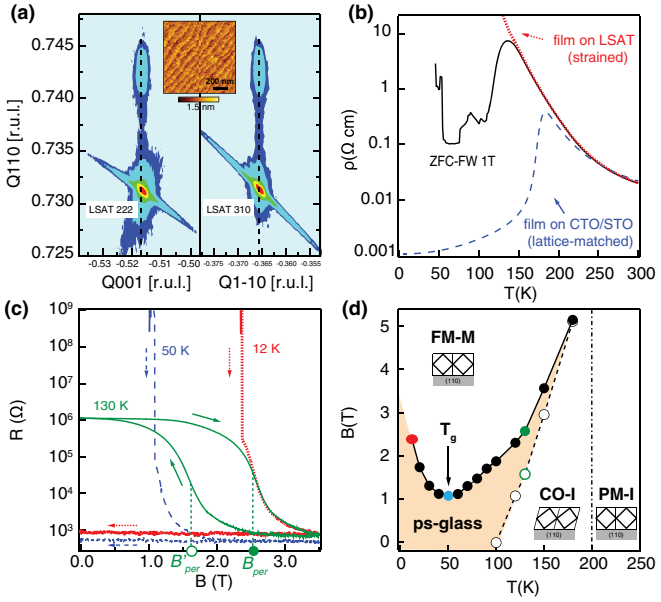

FIG. 1 (color online). (a) Reciprocal space map of the PCSMO film grown on LSAT. (b) Resistivity of the strained PCSMO/LSAT film (dotted red) and a relaxed film on the CTO/STO substrate (dashed blue). The solid black line was taken during field warming after ZFC with $B = 1$ T. (c) Magnetoresistance after ZFC to 12 K, 50 K, and 130 K. The full and empty circles indicate B_{per}/B'_{per} for the forward and backward sweeps, respectively. (d) B-T phase diagram constructed from B_{per} and B'_{per} at various temperatures. The insets show schematic views of the film on LSAT (110) in each phase. Both the PM-I and FM-M phases have cubic structures, while the CO-I phase is distorted orthorhombic.

In order to identify the glassy PS state, we constructed the B-T phase diagram of the PCSMO film on LSAT using isothermal magnetoresistive curves obtained after ZFC to various temperatures. Examples of such curves at 12, 50, and 130 K are given in Fig. 1(c). For $T < 50$ K, the magnetoresistance curves with increasing B fields show a sharp transition to the metallic phase (percolation transition), while the opposite is not seen when sweeping back to zero field [dotted-red and dashed-blue curves in Fig. 1(c)]. At temperatures higher than 50 K, the transition is smooth and the resistance returns back to the original value with a hysteresis after sweeping back of the fields (solid-green curve). The B field at the percolation point during the forward sweeping (B_{per}) gradually reduces from 12 K to 50 K and increases again at higher temperature. At $T > 100$ K, the backward sweeping curve shows a return to the high resistance state at B'_{per}. The B_{per} and B'_{per} data points at various temperatures enclose the glasslike region (orange shaded region) on the B-T phase diagram in Fig. 1(d). Outside this region, either the FM-M or CO-I states dominate the system, while inside, a glassy mixture of the FM-M and supercooled CO-I states is expected. In addition, the minimum B_{per} at 50 K indicates the freezing point of the PS glass [8], i.e., the glass transition temperature, T_g.

Microscopic PS of manganites can be readily observed by MIM [19], which functions by sending a 1-GHz microwave signal into a coaxial cantilever probe [26] and measuring the nanoscale sample impedance. Figure 2(a) shows a schematic of the cryogenic MIM measurement [27] (top) and the equivalent lumped-element circuit (bottom). The real and imaginary parts of the MIM outputs contain local conductivity information of the sample, with a spatial resolution down to 50 nm. Mn_3O_4 precipitates [28], which are always insulating within our temperature and field ranges, are present on the sample surface and conveniently serve as landmarks. For this study, the MIM response in the imaginary channel, which is proportional to the tip-sample capacitance [29], is sufficient to identify the Mn_3O_4, CO-I, and FM-M regions. We use false color map to label each region as black, red, and yellow, respectively [30].

We investigated the low-temperature states after cooling at different rates. A fast cool down (FCD) at 8 K/min and a slow cool down (SCD) at 0.3 K/min were employed to reach specific temperatures at which the images were taken. Figures 2(b) and 2(c) show representative images at 12 K for FCD and SCD, respectively. The substantial FM-M fraction in the nominally insulating film is striking. Indeed, careful image analysis [Fig. 1 and Fig. 2(g)] shows that the

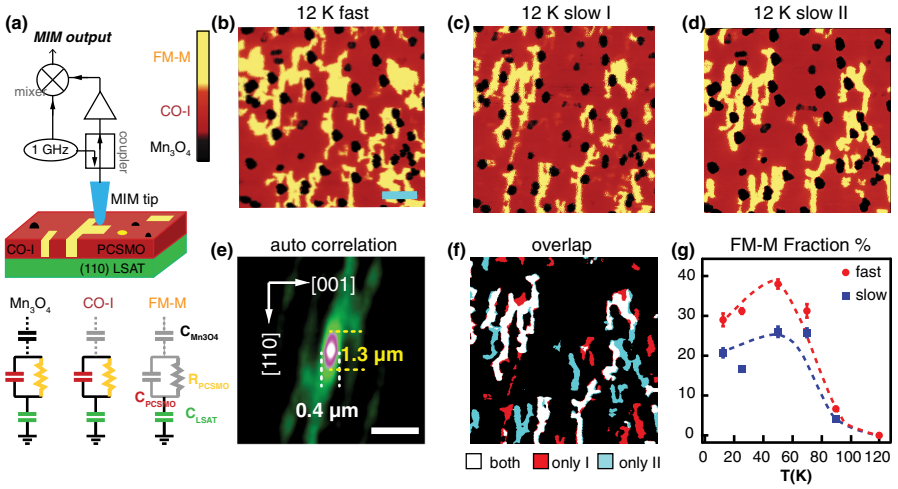

FIG. 2 (color online). (a) (top) Schematic of the MIM setup and (bottom) the equivalent circuit of the tip-PCSMO film interaction. The MIM responses on the Mn_3O_4, CO-I, and FM-M regions are colored in black, red, and yellow, respectively. (b)–(d) From left to right, MIM images at 12 K after FCD, and after two SCDs. (e) Autocorrelation analysis of the SCD-I image, illustrating the preferred alignment of FM-M domains along the axis of the substrate [1–10]. (f) Overlay of the domains from the two SCDs. All scale bars are 2 μm. (g) FM-M fractions of the two processes as a function of temperature.

FM-M states can occupy up to 40% of the sample when cooling at zero field. This result indicates a strong competition between the two states even at zero B field. Interestingly, the presence of these FM-M clusters is not measurable in either the resistivity [Fig. 1(b)] or the magnetization (Supplemental Material [24]). The former is expected for a FM-M faction below the percolation threshold [19], and the latter is due to the random orientation of macrospins from the FM-M clusters [31].

By considering the crystal structure of each phase [Fig. 1(d)], we can explain how a slow cooling rate leads to fewer FM-M domains. At 200 K, the transition from PM-I to CO-I is accompanied by a structural phase transition [21,32]. This process is likely to be highly viscous, and some PM-I regions may directly enter the FM-M rather than the CO-I phase; thus, more FM-M domains are found at low temperature under a fast cooling process. Furthermore, in Fig. 2(e), the autocorrelation analysis of the SCD images shows the tendency of FM-M domains to elongate along the [1–10] axis of the substrate, suggesting stronger influences from the local domain structure [10,19]. In addition, compared to the metallic behavior in the unstrained film on the CTO/STO substrate, we believe that the PS glassy state in the strained film on a LSAT substrate is mainly induced by substrate elastic strain.

The SCD state has noticeably fewer FM-M domains than that after FCD. Interestingly, while the percentages of area occupied by the FM-M domains are about the same for the two identical SCDs, the MIM images show different FM-M domain configurations. In Fig. 2(f), two SCD images are overlaid for comparison, with about 50% of the FM-M domains appearing at different locations. The overlapped domains are likely pinned by intrinsic defects [19], while the random appearance of the rest is a clear evidence of the nonergodicity.

The observed PS states are far from being static, as shown in the relaxation of the PS state after zero-field cooling [4,5,12]. Before each cooling, the sample was warmed up to 250 K, above the charge-order temperature T_{co}, to remove the impact of any prior history. The cooling rate was kept at 8 K/ min. Figure 3(a) shows images after ZFC to various temperatures above and below T_g. Repeated scans on the same area show drastic changes in the PS at $T > 20$ K [Fig. 3(b)]. After a waiting time of 4 hours at 50 K, the FM-M domains grew from 40% to 50%. More importantly, many FM-M domains appeared at different locations even though the change in FM-M percentage was small. In other words, a simple measure of the areal fraction [Fig. 3(c), inset] cannot capture the dynamics here. Such dynamical behavior can be illustrated by overlapping the FM-M domains before and after the holding period at 70 K, as shown in Fig. 3(d). On the other hand, the images taken at 12 K show no change after 18 hours. The microscopic rearrangement can be numerically studied by calculating the cross-correlation coefficient r_{xy} between the images before and after the 4-hour interval. As shown in the inset of Fig. 3(c), r_{xy} is small ($\sim$0.5) at high temperatures but rapidly rises towards 1 below 20 K, a vivid demonstration of the freezing of the PS glass at this temperature [8].

We further investigated the dynamic switching of the PS glass state from the FM-M to CO-I by monitoring the relaxation after removing an external B field [5] [Fig. 4(a)]. The sample was again prepared by ZFC to the desired T before turning on the B field. A field of 2.4 T induced a significant portion of FM-M phases at all temperatures. Immediately after its removal, however, very different behaviors occurred at different temperatures. For $T < T_g$, the PS was frozen with virtually no change in its configuration 18 hours after switching off the field. In contrast,

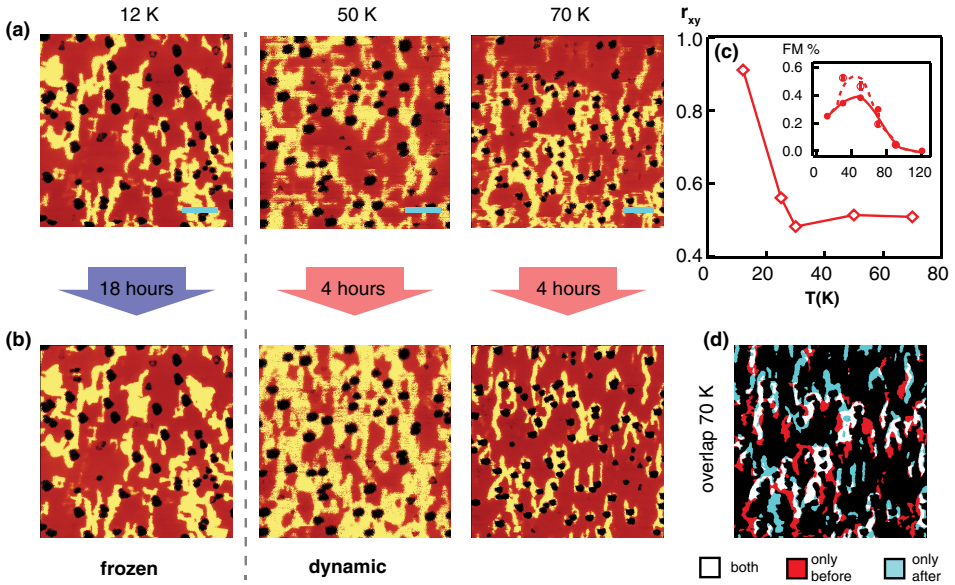

FIG. 3 (color online). (a),(b) MIM images after (a) FCD and (b) waiting for several hours at 12, 50, and 70 K, respectively. (c) Cross-correlation coefficient r_{xy} as a function of temperature, showing a sharp jump of r_{xy} at $T_g \sim 20$ K. The inset summarizes the FM-M fractions before (solid) and after (empty circle) a holding time of 4 hours. (d) Overlap of the two images at 70 K, showing the emergence of a number of new FM domains, and the disappearance of previously existing domains.

dynamic behavior was observed at higher temperatures. At 50 K, no obvious change was observed right after turning off B, while the insulating regions expanded after one day. The relaxation was much faster at 70 K, where large changes happened right after field removal and continued for several hours. For high enough $T = 120$ K, the relaxation back to the zero-field state was faster than our imaging time; hence, little variation can be seen after another hour of waiting. Figure 4(b) summarizes the measured FM-M fraction throughout this process. Using the FM-M fraction as a function of time [Fig. 4(c), inset] and assuming a logarithmic time dependence [4], we can extract the relaxation time as a function of temperature (Supplemental Material [24]). As seen in Fig. 3(c), the relaxation time, on the order of several hours, diverges when approaching T_g. On the other hand, the

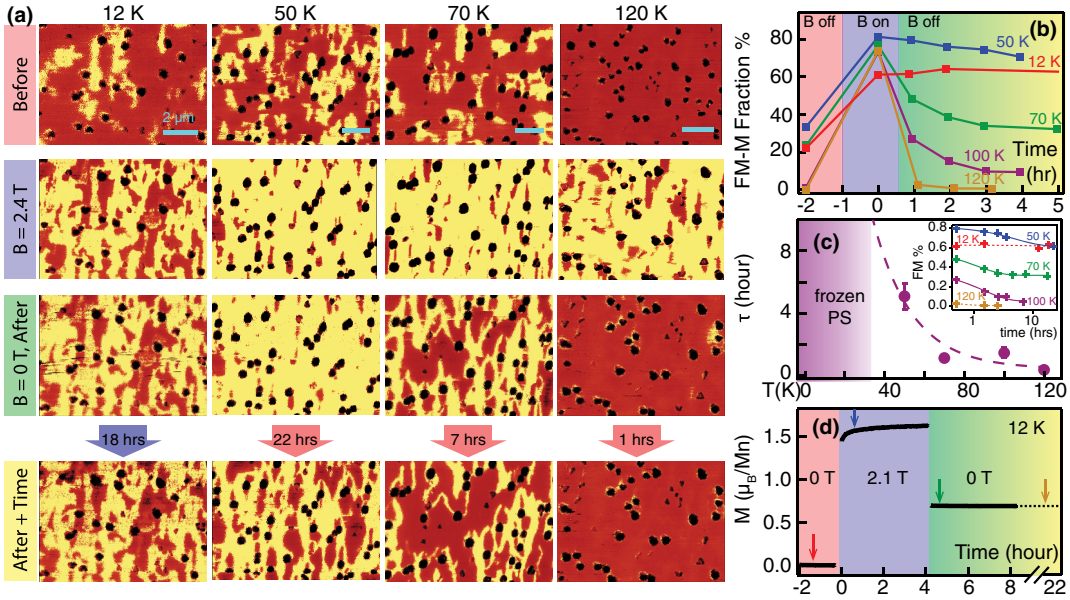

FIG. 4 (color online). (a) MIM images taken at $B = 0$ T (before), $B = 2.4$ T, $B = 0$ T (after), and after several hours at the same condition (after + time) at $T = 12$, 50, 70, and 120 K, respectively. All scale bars are 2 μm. (b) FM-M vs time showing the fraction before, at $B = 2.4$ T, turning of the B field at different T. (c) Relaxation time as a function of temperature calculated from an exponential fit of FM-M vs time. (d) Magnetization as a function of time. The B field is applied at time zero and removed after 4 hours. The arrows indicate where the MIM images were taken.

magnetization dropped by almost half [Fig. 4(d)] immediately upon field removal even at 12 K. In other words, a sizable amount of spins in the FM-M clusters are still able to randomize even though the cluster itself is frozen.

In summary, microwave microscopy study of PCSMO film on LSAT reveals a PS texture with nonergodicity and relaxation behavior, which are the key hallmarks of a glassy state. The glassiness is driven by phase competition and is strongly influenced by the tensile strain from the substrate, resulting in preferential alignment of the FM-M domains. The microscopic configurations of PS states are highly dependent on the cooling history and differ even after the same cooling process. The PS exhibits dynamic behavior such as growing and shrinking of the FM-M domains, but the relaxation virtually stops below the freezing temperature. The freezing behavior is seen in the rapid growth in cross-correlation coefficient from the time-dependence images and the relaxation time constant from the ferromagnetic domain areal fraction. By demonstrating a route to visualize and quantify quantum glassy states, this Letter should facilitate further investigation into electronic phase separation systems.

We thank Daniel S. Fisher for stimulating discussions. The measurement work done at Stanford University is supported by NSF Grants No. DMR-1305731 and No. DMR-0906027, and the probe development is supported by the Center of Probing the Nanoscale NSF Grant No. PHY-0425897 and the Gordon and Betty Moore Foundation through Grant No. GBMF3133 to Z. X. S. The work done in RIKEN was supported by the JSPS FIRST program. This work was also supported by Suranaree University of Technology (SUT), and the Office of the Higher Education Commission under the National Research University (NRU) project. This work was supported by the Natural Science Foundation of China, Grant No. 11574316, U1532155, and the One Thousand Talents Program of China.

W. K. and Z. S. contributed equally to this work.

*Corresponding author.
zxshen@stanford.edu

[1] P. G. Debenedetti and F. H. Stillinger, Nature (London) **410**, 259 (2001).
[2] E. Dagotto, T. Hotta, and A. Moreo, Phys. Rep. **344**, 1 (2001).
[3] E. Dagotto, J. Burgy, and A. Moreo, Solid State Commun. **126**, 9 (2003).
[4] M. Sirena, L. B. Steren, and J. Guimpel, Phys. Rev. B **64**, 104409 (2001).
[5] J. López, P. N. Lisboa-Filho, W. A. C. Passos, W. A. Ortiz, F. M. Araujo-Moreira, O. F. de Lima, D. Schaniel, and K. Ghosh, Phys. Rev. B **63**, 224422 (2001).
[6] L. Ghivelder and F. Parisi, Phys. Rev. B **71**, 184425 (2005).
[7] P. A. Sharma, S. B. Kim, T. Y. Koo, S. Guha, and S.-W. Cheong, Phys. Rev. B **71**, 224416 (2005).
[8] P. A. Sharma, S. El-Khatib, I. Mihut, J. B. Betts, A. Migliori, S. B. Kim, S. Guha, and S.-W. Cheong, Phys. Rev. B **78**, 134205 (2008).
[9] Y. Tomioka and Y. Tokura, Phys. Rev. B **70**, 014432 (2004).
[10] K. H. Ahn, T. Lookman, and A. R. Bishop, Nature (London) **428**, 401 (2004).
[11] J. Sacanell, F. Parisi, J. C. P. Campoy, and L. Ghivelder, Phys. Rev. B **73**, 014403 (2006).
[12] I. G. Deac, S. V. Diaz, B. G. Kim, S.-W. Cheong, and P. Schiffer, Phys. Rev. B **65**, 174426 (2002).
[13] T. Z. Ward, Z. Gai, H. W. Guo, L. F. Yin, and J. Shen, Phys. Rev. B **83**, 125125 (2011).
[14] M. Fäth, S. Freisem, A. A. Menovsky, Y. Tomioka, J. Aarts, and J. A. Mydosh, Science **285**, 1540 (1999).
[15] J. Q. He, V. V. Volkov, T. Asaka, S. Chaudhuri, R. C. Budhani, and Y. Zhu, Phys. Rev. B **82**, 224404 (2010).
[16] M. H. Burkhardt, M. A. Hossain, S. Sarkar, Y.-D. Chuang, A. G. Cruz Gonzalez, A. Doran, A. Scholl, A. T. Young, N. Tahir, Y. J. Choi, S.-W. Cheong, H. A. Dürr, and J. Stöhr, Phys. Rev. Lett. **108**, 237202 (2012).
[17] W. Wu, C. Israel, N. Hur, S. Park, S.-W. Cheong, and A. de Lozanne, Nat. Mater. **5**, 881 (2006).
[18] R. Rawat, P. Kushwaha, D. K. Mishra, and V. G. Sathe, Phys. Rev. B **87**, 064412 (2013).
[19] K. Lai, M. Nakamura, W. Kundhikanjana, M. Kawasaki, Y. Tokura, M. A. Kelly, and Z.-X. Shen, Science **329**, 190 (2010).
[20] N. Takubo, Y. Ogimoto, M. Nakamura, H. Tamaru, M. Izumi, and K. Miyano, Phys. Rev. Lett. **95**, 017404 (2005).
[21] Y. Wakabayashi, N. Takubo, K. Miyano, and H. Sawa, Eur. Phys. J. Spec. Top. **167**, 67 (2009).
[22] Z. Sheng, M. Nakamura, F. Kagawa, M. Kawasaki, and Y. Tokura, Nat. Commun. **3**, 944 (2012).
[23] D. Okuyama, M. Nakamura, Y. Wakabayashi, H. Itoh, R. Kumai, H. Yamada, Y. Taguchi, T. Arima, M. Kawasaki, and Y. Tokura, Appl. Phys. Lett. **95**, 152502 (2009).
[24] See Supplemental Material at http://link.aps.org/supplemental/10.1103/PhysRevLett.115.265701 for information about the properties of the PCSMO films on LSAT and CTO/STO substrates image analysis methods, relaxation time calculation, and images from the paper in a gradual color scale.
[25] Y. Tomioka and Y. Tokura, Phys. Rev. B **66**, 104416 (2002).
[26] Y. Yang, K. Lai, Q. Tang, W. Kundhikanjana, M. A. Kelly, K. Zhang, Z. X. Shen, and X. Li, J. Micromech. Microeng. **22**, 115040 (2012).
[27] W. Kundhikanjana, K. Lai, M. A. Kelly, and Z.-X. Shen, Rev. Sci. Instrum. **82**, 033705 (2011).
[28] T. Higuchi, T. Yajima, L. F. Kourkoutis, Y. Hikita, N. Nakagawa, D. A. Muller, and H. Y. Hwang, Appl. Phys. Lett. **95**, 043112 (2009).
[29] K. Lai, W. Kundhikanjana, M. A. Kelly, and Z. X. Shen, Rev. Sci. Instrum. **79**, 063703 (2008).
[30] In fact, a large metallic domain gives a small impedance compared to a small domain, and, thus, a higher MIM signal. Therefore, different domains would have slightly different colors in a color scale with gradual color change depending on the size of the domains. Here, we present the images in the three-level color scale for simplicity. Images in the gradual color scale are provided in the Supplemental Material [24].
[31] M. Uehara, S. Mori, C. H. Chen, and S.-W. Cheong, Nature (London) **399**, 560 (1999).
[32] Y. Wakabayashi, H. Sawa, N. Takubo, M. Nakamura, Y. Ogimoto, and K. Miyano, J. Phys. Conf. Ser. **211**, 012004 (2010).